Photonic Millimeter-Wave System for High-Capacity Wireless Communications

Timothy P. McKenna, Jeffrey A. Nanzer, and Thomas R. Clark Jr.

ABSTRACT

The demand for high-speed wireless communications continues to grow rapidly, and future wireless systems will require data rates of 10 Gb/s and higher. Applications include wireless infrastructure backhaul and wireless personal area networking. Millimeter-wave systems using photonics techniques are suited for high-speed communications because of the large bandwidths that are possible, the favorable radiation propagation, and the ability to transport broadband millimeter-wave signals over long distances using optical fiber. This article outlines recent work on a photonics-enabled millimeter-wave communications system operating in the W-band with a 10-Gb/s data rate. Current research includes millimeter-wave phased-array technology and integration approaches.

INTRODUCTION

The term *millimeter-wave*, commonly abbreviated mm-wave, nominally refers to the frequency range of 30–300 GHz (wavelengths of the range 1–10 mm), corresponds to the extremely high-frequency band of the International Telecommunication Union band designations, and extends from the Ka-band through the mm-wave band of the IEEE standard letter band designations (see Table 1). Millimeter-wave frequencies have long been of interest for remote sensing because of their ability to achieve high spatial resolution with small physical apertures. Applications in missile guidance radar systems and radio astronomy extend back decades[1,2] when technologies focused on W-band (75–110 GHz) frequencies, in particular near 94 GHz where atmospheric absorption is low. Many devices were developed for these applications; however, compared with lower-frequency devices, the performance of mm-wave components and systems was lacking in terms of noise, efficiency, and cost.

The drive for increased data rates, and thus increased bandwidth, in communications systems, coupled with the need for improved spatial resolution in remote sensing systems, has driven mm-wave technologies to the point at which improved performance, greater availability, and lower cost of devices have allowed for mainstream applications. Wireless communications systems today generally operate at lower microwave frequencies where components have better performance at low cost. Typical Wi-Fi (IEEE 802.11) networks operate in the 2.4- and 5-GHz bands, while cellular telephone systems typically operate below 3.0 GHz. However, the bandwidth at these frequencies is constrained compared with that at mm-wave frequencies, and future systems will require bandwidth exceeding what is available at microwave frequencies. A recently defined high-bandwidth wideband personal area network standard (IEEE 802.15.3c) specifies wireless data rates up to 5.28 Gb/s operating in

Table 1. IEEE microwave and mm-wave band designations

Band Designation	Frequency Range (GHz)
L	1–2
S	2–4
C	4–8
X	8–12
Ku	12–18
K	18–26.5
Ka	26.5–40
V	40–75
W	75–110
mm-wave	30–300

the unlicensed 57- to 64-GHz band. Communications systems operating in the V-band (40–75 GHz) are thus actively being pursued, as are systems in the W-band (75–110 GHz). Meanwhile, mm-wave imaging sensors for security applications have already been deployed in large volumes in airports and other checkpoints.

Although many advances in mm-wave technologies have been made, future applications require further technological development. Electronic mm-wave devices are able to support some of the requirements of developing systems; however, limitations exist that are challenging to overcome. For example, generating and modulating sufficiently low-noise mm-wave signals to enable high-data-rate communications is difficult using electronic techniques. Electronic oscillators generate stable signals with low phase noise at megahertz frequencies that can then be frequency multiplied up to gigahertz frequencies, but the phase noise power of the output frequency increases by 6 dB with every doubling in frequency, which greatly reduces the noise performance at high mm-wave frequencies. Millimeter-wave diode oscillators such as IMPATT and Gunn oscillators can generate high powers across wide frequency ranges; however, they generally have poor noise performance. Upconversion and downconversion of waveforms to and from the mm-wave carrier frequency using electronic heterodyne architectures can be limited by the finite bandwidths that mixers can support, and the amplitude and phase can vary significantly across the bandwidth. Loss in mm-wave waveguide (~3 dB/m in WR-10 at 80 GHz) and planar transmission lines (~0.1 dB/mm for 45-μm-thick benzocyclobutene substrate at 80 GHz) are sufficiently high to severely restrict the transport distance.

Photonic techniques have made significant advances in recent years and offer approaches to reduce or eliminate the drawbacks associated with current electronic mm-wave technologies. Techniques such as photonic signal generation, signal upconversion and downconversion, and optical remoting offer advantages in performance and architecture over electronic techniques.

MOTIVATIONS FOR MILLIMETER-WAVE TECHNOLOGY

Compared with systems operating at lower frequencies, mm-wave wireless systems have important benefits. Because of the shorter wavelengths of the signals, components and systems can be made smaller and more compact than microwave systems. The antenna aperture in particular can be made physically much smaller while maintaining the same performance such as gain and directivity. For example, a 10-GHz Cassegrain reflector antenna with 48-dBi gain requires a primary reflector with a diameter of approximately 3 m, whereas a 94-GHz Cassegrain with the same gain requires a primary reflector with a diameter of approximately 0.3 m.

Another significant benefit of operating wireless systems at mm-wave frequencies is the large bandwidths that are available. Because the fractional bandwidth of standard electronic designs is relatively constant over frequency, wider bandwidths, and thus increased data rates, can be achieved at mm-wave frequencies. The primary drawback for long-range mm-wave propagation is the attenuation of the signal when propagating through the atmosphere. Figure 1 shows the atmospheric attenuation at sea level as a function of frequency. The overall trend is an increase in absorption as the frequency increases, and the high absorption bands are due to absorption by water or oxygen molecules. The areas in between these bands are referred to as atmospheric windows, where long-range propagation is possible. The absorption plot changes with temperature, humidity, and weather conditions.

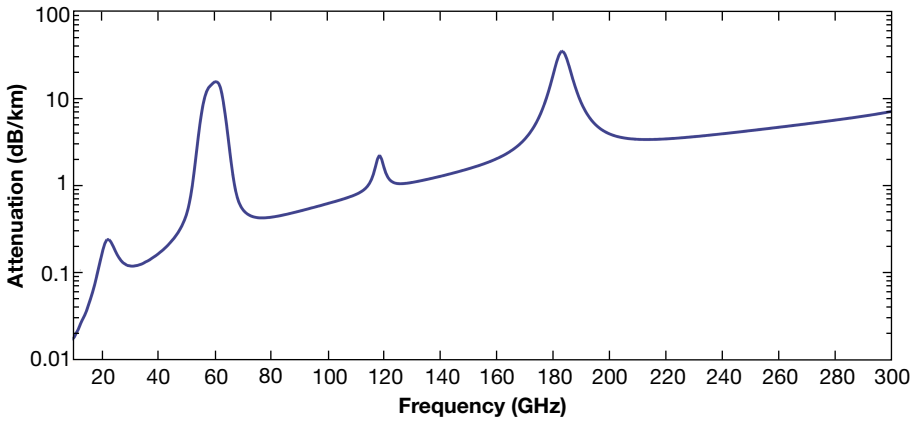

Figure 1. Atmospheric absorption at sea level as a function of frequency.

Atmospheric absorption is not the only factor to consider when designing mm-wave wireless systems. In particular, the required data rate for communication systems should also determine the best frequency band of operation. An optimal band can be determined by considering the channel capacity (equivalent to the maximum data rate) using Shannon's theorem: $C = B \log_2(1 + SNR)$, where C is the channel capacity, B is the available bandwidth, and SNR is the signal-to-noise ratio. The size of the system is also an important consideration. In the following analysis to determine the optimal frequency band, the antenna diameter is fixed at 0.3 m (12 in.), and a Cassegrain reflector is assumed. To find the optimal frequency, the transmit power multiplied by the SNR required to achieve the specified capacity forms the figure of merit (FOM), which is a difficulty parameter with low values being less difficult. Figure 2 shows the results of an evaluation to achieve capacities ranging from 1 Gb/s to 100 Gb/s for a 50-km link with a 10% fractional bandwidth assuming the atmospheric conditions described in Fig. 1. For capacities 10 Gb/s and higher, the optimal region for operation occurs in the W-band (75–110 GHz) because of the lower SNR requirements than at the lower frequencies. For lower capacities, the 30- to 50-GHz band is preferable because of lower atmospheric attenuation.

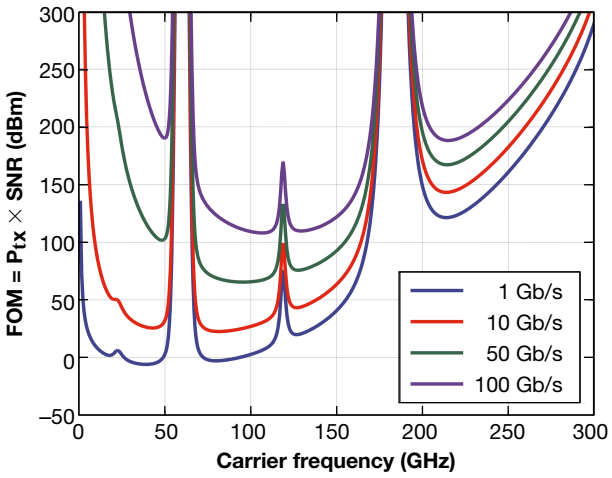

Figure 2. Optimal carrier frequency vs. capacity analysis for link range of 50 km, antenna diameter of 12 in., and 10% fractional bandwidth.

MOTIVATIONS FOR PHOTONIC TECHNOLOGY

Systems incorporating photonics technology offer a number of benefits over traditional all-electronic implementations. Particularly advantageous is the broad bandwidth capability of photonics, which can be used for photonic frequency synthesis[3] as well as photonic upconversion[4] and downconversion,[5,6] as shown in the photonics-enabled mm-wave transceiver in Fig. 3. Low-loss signal transport through photonic remoting and photonic interfacing of subsystems also allows preferential hardware distribution, packaging, and efficient interconnections.[7] Additionally, photonic implementations support the linearity and SNR requirements needed for spectrally efficient modulation formats. Over the past decade, optical components have been developed to support complex modulation formats for fiber optic telecommunications with data rates far exceeding those of wireless systems.

Photonic remoting and signal transport for microwave and mm-wave systems have long been seen as advantages for future systems. The attenuation over optical fiber is near 0.2 dB/km, and the RF operating frequency is largely irrelevant for mm-wave frequencies

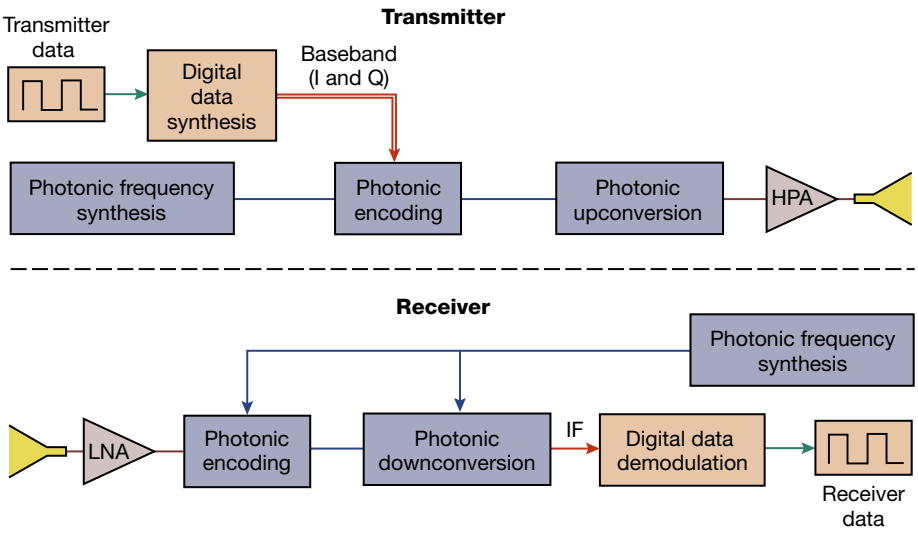

Figure 3. Photonics-enabled transmitter and receiver block diagrams. HPA, high-power amplifier.

as the signals are transported on optical carriers (typically around 193 THz for the lowest fiber loss region). Even short subsystem interfaces in waveguide and planar transmission lines require all desired circuit functions to be closely integrated to maintain signal integrity. High-performance systems of the future will be possible by using photonic techniques such as fiber remoting, signal generation, signal conditioning, and frequency translation, as described in the following section.

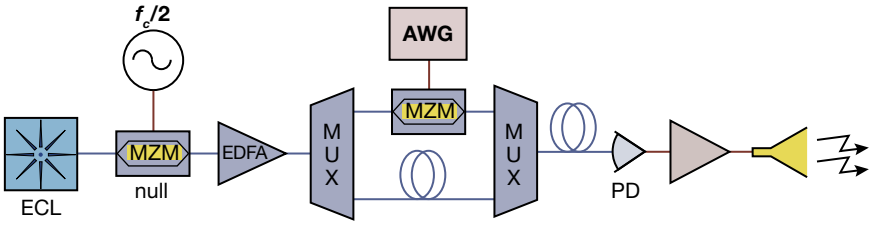

Figure 4. Transmit architecture. All fiber is polarization maintaining. AWG, arbitrary waveform generator; ECL, external cavity laser; EDFA, erbium-doped fiber amplifier; MUX, multiplexer/demultiplexer; MZM, Mach–Zehnder modulator; PD, photodiode. (Reproduced from Ref. 8.)

PHOTONIC MILLIMETER-WAVE SYSTEM

In this section we describe the experimental implementation of a photonic mm-wave wireless communications system operating in the W-band. Our system included significant subsystem signal transport over optical fiber to minimize the required hardware at the antenna, as well as photonic mm-wave signal generation and data upconversion. We first discuss the photonic mm-wave transmitter and receiver and then discuss an on-campus outdoor demonstration.

Transmitter

Photonic techniques generate the mm-wave transmit signal using standard fiber optic telecommunications

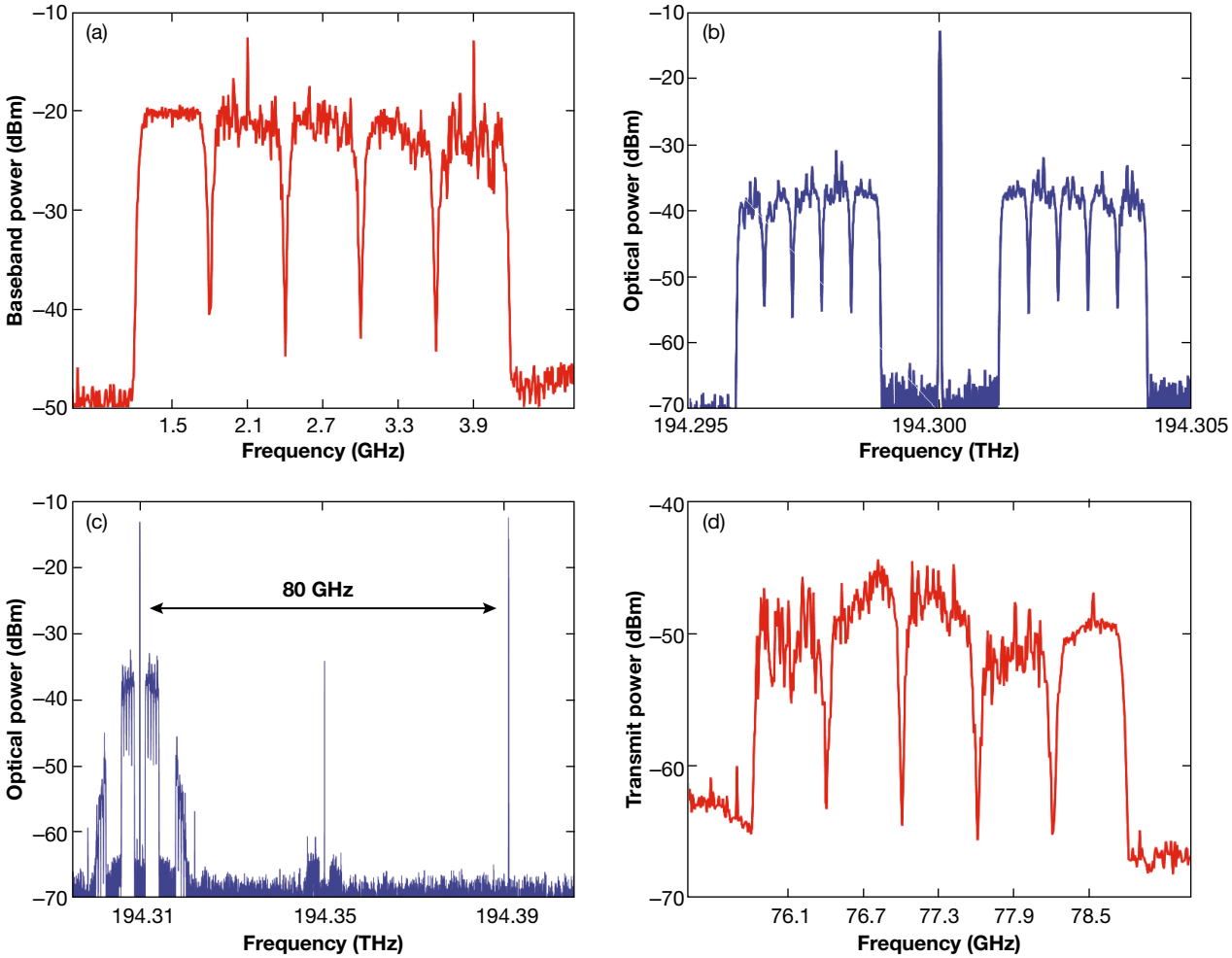

Figure 5. (a) Baseband electrical signal. (b) Baseband data encoded on the optical carrier. (c) Optical signal incident on the photodiode. (d) Transmit mm-wave spectrum. (Reproduced from Ref. 8.)

components and a high-speed photodiode. The transmitter's operation relies on interfering two optical tones of different frequencies on a high-speed photodiode to generate the mm-wave signal. Figure 4 shows a diagram of the transmitter.

To photonically generate two optical tones of a specified frequency separation, an external cavity laser serves as input to a lithium niobate electro-optic modulator that is biased at its minimum transmission point. A single RF tone at $f_c/2$ drives the modulator, which produces a suppressed optical carrier and optical sidebands spaced by integer multiples of the RF drive frequency. The second harmonic term produces an electrical signal at the desired carrier frequency given by

$$E_{2H} = t_m P_0 J_2\left(\frac{V_p \pi}{V_\pi}\right)\sin\left(2\pi f_c t + \frac{\pi}{2}\right), \qquad (1)$$

where t^m is the modulator transmission factor, P^0 is the laser source power, J^2 is the Bessel function of the first kind of order 2, V^p is the amplitude in volts of the RF driving source, and V_π is the voltage required to induce a π phase shift in the modulator. Driving with $V^p = 0.97 \cdot V_\pi$ maximizes the power of the second harmonic sidebands. After optical amplification, the two dominant optical tones separated by frequency f^c are filtered and enter the signal encoding stage. In the signal encoding stage, one optical sideband is encoded, and the other sideband remains unmodulated to serve as the reference tone for the upconversion process. The data signal is modulated with a lithium niobate modulator biased at quadrature. The 10-Gb/s data signal consists of five 2-Gb/s 16-QAM subcarriers resulting in a total occupied bandwidth of 3 GHz. A wavelength multiplexer recombines the modulated signal with the optical tone, and the two signals interfere on a high-speed photodiode to generate the mm-wave signal. The output of the photodiode is amplified to a power level of −10.2 dBm and radiated from a Cassegrain antenna with a gain of 49.9 dBi and a 3-dB beamwidth of 0.55° at 80 GHz. All sidelobes are at least 20 dB below the main lobe, and the measured transmit SNR is 19.1 dB, limited by the measurement instrument. Figure 5a shows the baseband electrical signal before modulating the optical carrier. Figure 5b shows the

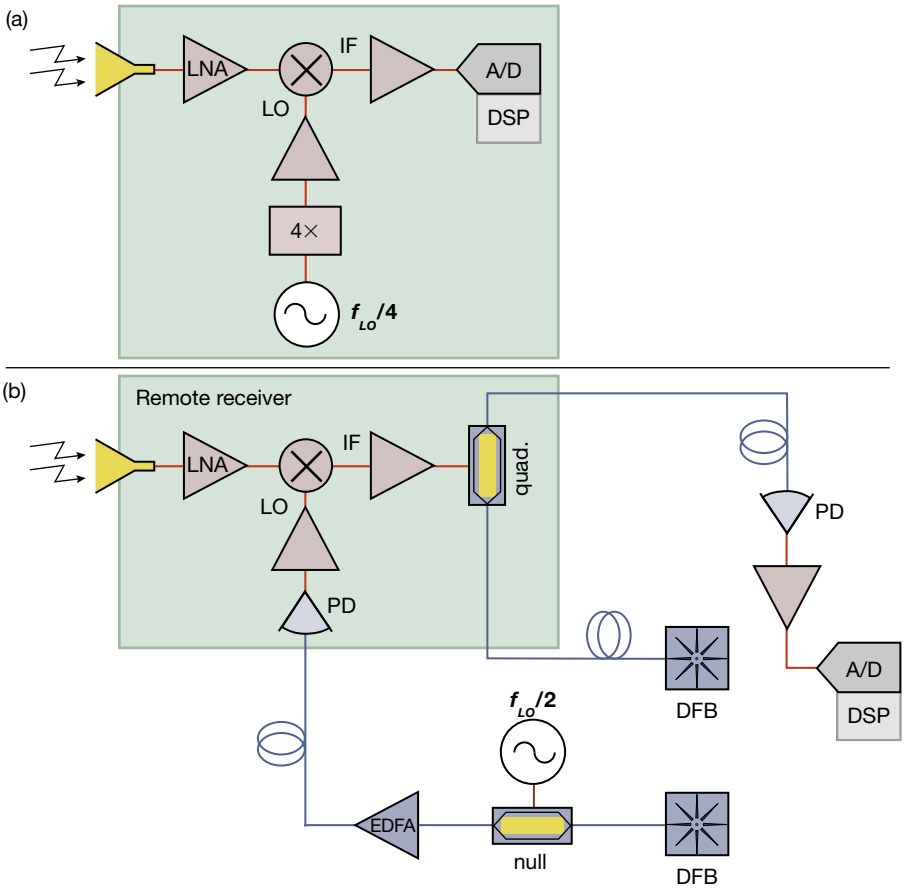

Figure 6. (a) All-electronic receiver configuration. (b) Photonics-assisted receiver configuration. 4×, four times frequency multiplier; ADC, analog-to-digital converter; DFB, distributed feedback laser; EDFA, erbium-doped fiber amplifier; MZM, Mach–Zehnder modulator; PD, photodiode. (Reproduced from Ref. 8.)

modulated optical carrier, and Fig. 5c shows the optical spectrum of the signal incident on the photodiode. Figure 5d shows the resulting mm-wave data signal after amplification.

Receiver

Figure 6 shows the two receiver configurations used in the outdoor experiment. A Cassegrain antenna with a gain of 50 dBi and a 3-dB beamwidth of 0.60° at 80 GHz receives the wireless signal. A low-noise amplifier (LNA) amplifies the received signal before mixing with the local oscillator (LO) signal using a balanced Schottky diode mixer. Figure 6a shows the all-electronic receiver where electronic frequency multiplication generates the LO that drives the mixer at a level greater than 12 dBm. In the configuration of Fig. 6a, digitization of the intermediate frequency (IF) signal occurs close to the antenna aperture to avoid attenuation by a long coaxial cable.

Figure 6b shows the photonics-enabled receiver that includes techniques to allow for LO generation and digitization to occur away from the antenna aperture. Photonic LO generation uses the same suppressed carrier technique as the mm-wave carrier generation at the transmitter, but the optical tones remain unmodulated to provide a clean LO drive signal. To remote the IF signal to the digitizing hardware, a photonic link[9] transports the IF signal from the mixer to the digitizer. The photonic link has amplification at the input and output, and measured performance of the link's third-order input intercept point, gain, and noise figure are −19.9 dBm, 38.1 dB, and 13.0 dB, respectively.

A 50-GS/s oscilloscope with a 20-GHz bandwidth digitizes the IF signal, and offline digital signal processing (DSP) performs filtering, channel equalization, and signal demodulation. Use of a field-programmable gate array offers a straightforward path to real-time demodulation.

As an estimate of the demonstrated link, we use the Friis transmission equation to predict received power for a given transmitted power in units of decibels. The received power is given by

$$P_r = P_t + G_t + G_r + 20\log\left(\frac{\lambda}{4\pi R}\right), \qquad (2)$$

where P^r is the received power; P^t is the transmitted power; G^t and G^r are the gains in dBi of the transmit and receive antennas, respectively; λ is the transmission wavelength; and R is the transmission range. Using our system parameters, a transmit power of −10.2 dBm results in a predicted receive power of −34.8 dBm over a range of 520 m at a 77-GHz center frequency. For our transmission test of less than 1 km with clear weather, atmospheric attenuation played a minimal role and was not used in the link budget.

Field Demonstration

To perform an outdoor link test, the antennas were placed on the rooftops of two buildings at the Johns Hopkins University Applied Physics Laboratory (APL). The system was tested over 520 m as shown in the aerial photograph in Fig. 7.

Figure 7. Aerial photograph of 520-m link range. (Reproduced from Ref. 8.)

The transmit mm-wave signal was generated approximately 100 m from the antenna and transported over optical fiber to the antenna. The only hardware at the antenna was the high-speed photodiode and mm-wave amplifiers as shown in Fig. 8.

For −10.2 dBm of transmitted power in the data sideband, −35.3 dBm of power was measured at the receiver. First, the system was tested with the electronic receiver shown in Fig. 6a. Figure 9a shows the resulting constellation of the 10-Gb/s signal for this received power. The error vector magnitudes (EVMs) of the subcarriers at the frequencies of 76.1, 76.7, 77.3, 77.9, and 78.5 GHz were measured to be 8.3%, 8.9%, 7.5%, 7.7%, and 7.1%, respectively, with the differences in EVM attributed to amplifier ripple.

Next, the photonics-assisted receiver shown in Fig. 6b was used to demonstrate high-data-rate communications. For the same transmit and receive powers, a data rate of 8 Gb/s is achieved by transmitting four subcarriers, each with a data rate of 2 Gb/s. The EVMs of the subcarriers at the transmit frequencies of 76.7, 77.3, 77.9, and 78.5 GHz were measured to be 14.1%, 13.7%, 13.5%, and 11.5%, respectively. Figure 9b shows the resulting constellation of the 8-Gb/s signal. The overall reduced sensitivity of the photonics-assisted receiver is attributed to the noise and dynamic range matching of the IF photonic link.

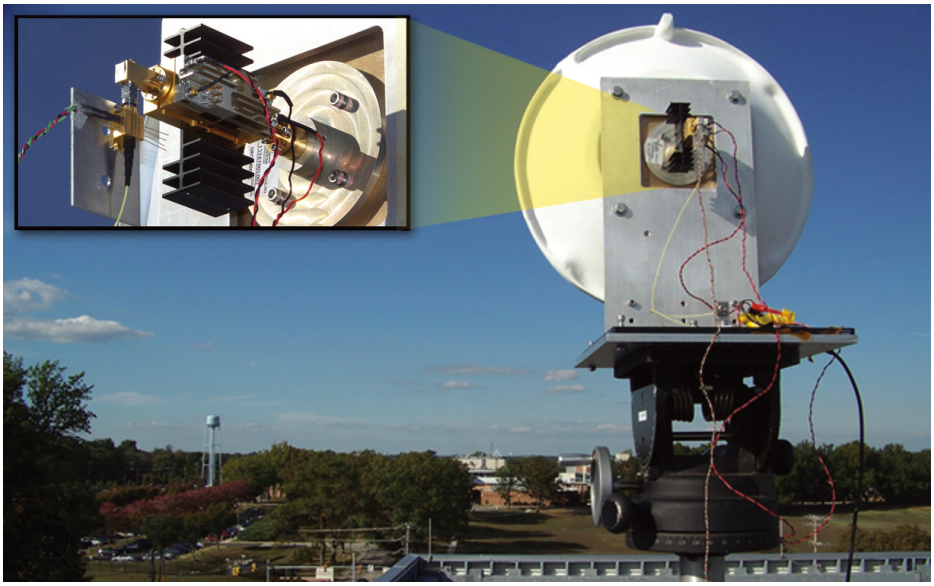

Figure 8. Photograph of transmit antenna and hardware. Inset, Close-up photograph of photodiode and amplifier chain. (Reproduced from Ref. 8.)

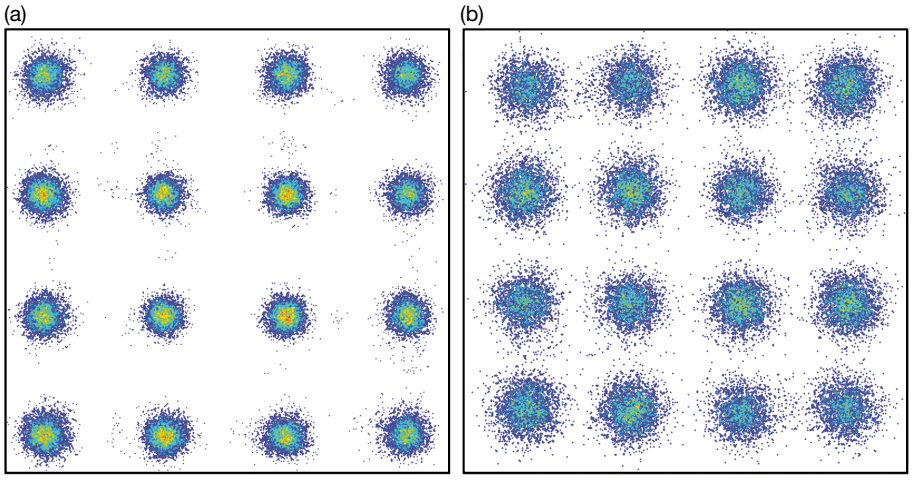

Figure 9. (a) 10-Gb/s 16-QAM data transmission with the all-electronic receiver. (b) 8-Gb/s 16-QAM data transmission with the photonics-assisted receiver. Symbols are aggregated over all subcarriers. (Reproduced from Ref. 8.)

CONTINUED WORK

All-Photonic Downconverting Receiver

In addition to upconversion, microwave photonic links can perform downconversion, making them suitable for communications receiver applications. Photonic links enable frequency translation without an electronic mixer or LO present near the antenna, which allows for minimal hardware at the transmit and receive apertures. High-dynamic-range microwave photonic downconverting links have been demonstrated[5,10,11] and photonic subsampling techniques have also been used for downconversion.[12–14]

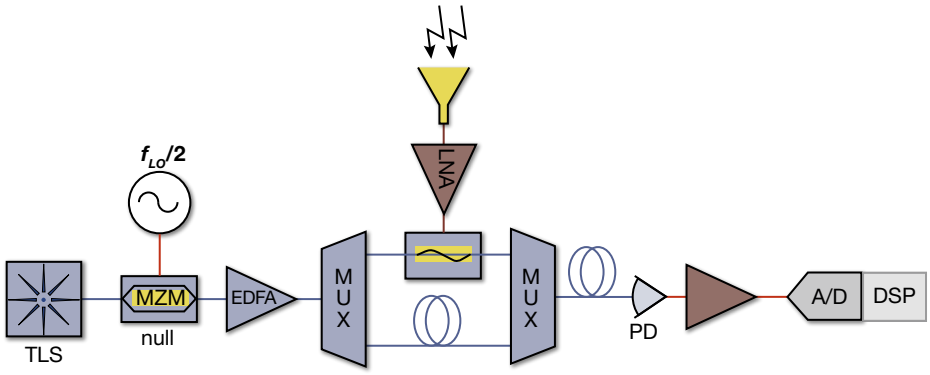

Figure 10. Receiver architecture. All fiber is polarization maintaining. A/D, analog-to-digital conversion; AWG, arbitrary waveform generator; EDFA, erbium-doped fiber amplifier; MUX, wavelength multiplexer; MZM, Mach–Zehnder modulator; PD, photodiode; TLS, tunable laser source. (Reproduced from Ref. 6.)

We have recently experimentally demonstrated a Ka-band downconverting receiver using phase modulation and an optical heterodyne process. Ten-Gb/s wireless data transmission using 16-QAM was demonstrated. Figure 10 shows a diagram of the receiver.

The sensitivity of the receiver is measured by placing the receiver 1 m from the transmitter and adjusting a waveguide attenuator placed before the receiver's LNA. Figure 11 shows the EVM as a function of received power. The inset in Fig. 11 shows the constellation for a received power of −42.92 dBm, which results in an equivalent bit error rate (BER) better than 10^{-9}.

A minimum received power of −50.4 dBm results in a 13.8% EVM, which corresponds to a BER of 4.6×10^{-4} assuming white Gaussian noise to be the primary impairment.[15] This BER is correctable using standard forward error correction codes.

Just as for the transmitter previously discussed, the modulator null-bias configuration used for optical two-tone generation provides optical phase coherence between the two optical tones because they are derived from a common laser source. Proper path length matching of the signal and reference fiber paths suppresses laser phase noise, and the 16-QAM constellation does not show noticeable rotation due to laser phase noise.

The gain of the downconverting photonic link, G, is given by

$$G = P_s P_r \left(\frac{\eta\pi}{V_\pi}\right)^2 R^2, \qquad (3)$$

where P^s and P^r are the optical powers incident on the photodiode in the signal and reference paths, respectively; η is the photodiode responsivity; V_π is the voltage required by the modulator to induce a π phase shift; and R is the input and output resistance (assumed to be matched). Using the receiver's parameters, the gain equation predicts a conversion loss of 16.9 dB, and a conversion loss of 18.0 dB was measured, with the difference likely due to a polarization offset introduced by optical fiber connectors. The gain equation provides the key parameters to minimize conversion loss. With photodiodes already available with greater than 0.8-A/W responsivity and power handling of 50 mA of photocurrent, lowering the phase modulator V_π is the most pressing improvement needed to reduce conversion loss and allow the receiver to scale to higher frequencies.

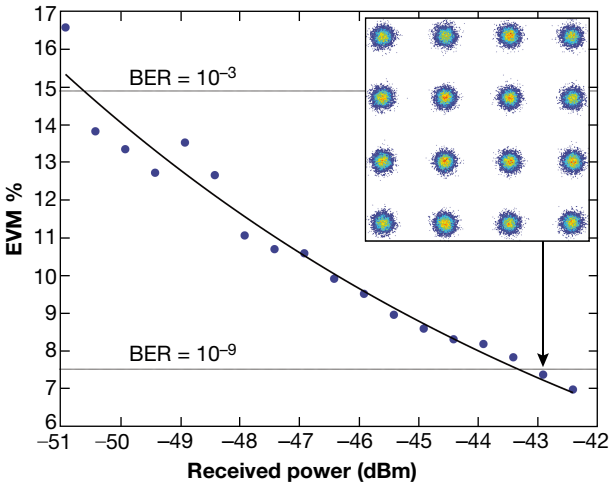

Figure 11. Plot of EVM as a function of received signal power. BERs of 10^{-3} and 10^{-9} are indicated. Inset, Signal constellation corresponds to a received power of −42.92 dBm. (Reproduced from Ref. 6.)

Photonic Millimeter-Wave Array

An important extension of the work described in the preceding section is the development of a photonically addressed and controlled mm-wave phased array. The short wavelengths of mm-wave radiation allow for highly directional beams with physically small aperture sizes. The small size and directivity of mm-wave apertures make beam steering important for applications with mobile transceivers. A phased antenna array allows for beam steering by adjusting the relative phases or time delays of the elements instead of physically adjusting the orientation of the antenna. Additionally, power-added gain due to multiple antenna elements can make phased-array techniques scale to high powers. In the following paragraphs, we describe our concept demonstration experiments for a transmit version of a photonics-enabled mm-wave array.

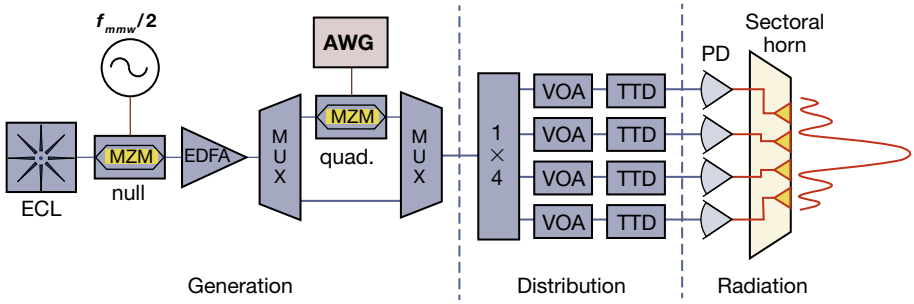

Figure 12. Schematic for mm-wave signal generation, distribution, and radiation. AWG, arbitrary waveform generator; ECL, external cavity laser; EDFA, erbium-doped fiber amplifier; MUX, multiplexer/demultiplexer; MZM, Mach–Zehnder modulator; PD, photodiode; VOA, variable optical attenuator. (Reproduced from Ref. 16.)

Figure 12 shows the architecture of the array. The generation stage is identical to the previously described and demonstrated transmitter. In the signal distribution stage, the signal is split into four single-mode fibers with each path corresponding to an antenna element. After the original signal is split, variable optical attenuators serve to power balance the signal paths. Next, photonic true-time delay (TTD) modules delay each path by an amount specified by the desired beam steering angle. The 4-bit TTD modules have nominal 1.5-ps step sizes and 24 ps of total delay available.

At each element a uni-traveling-carrier photodiode performs optical-to-electrical conversion. The photodiodes have 3-dB roll-offs greater than 90 GHz and responsivity greater than 0.5 A/W. The optical heterodyne upconversion process results in a mm-wave signal output from each photodiode that passes to each element of the antenna array. A 10-Gb/s data signal at a center frequency of 85 GHz radiates. The antenna has a simulated midband gain of about 18 dBi in the array dimension, with an array element spacing of 1.57 mm. At the receiver, after downmixing and amplification of the 12.32-GHz IF signal, a 50-GS/s oscilloscope with a bandwidth of 20 GHz records the waveform for offline processing.

To evaluate data transmission when beam steering, the receive antenna was placed 0.5 m from the transmit array, and the transmit power was held constant. Figure 13 shows the data transmission experiment data. First, 10-Gb/s data transmission at boresight (0°) was performed to serve as a baseline to evaluate any degradation due to steering. For a received signal power of −46.2 dBm, the EVM was 5.5%. Next, the TTD modules were programmed to provide delays that correspond to calculated beam steering angles of −35° and 35°. At −35°

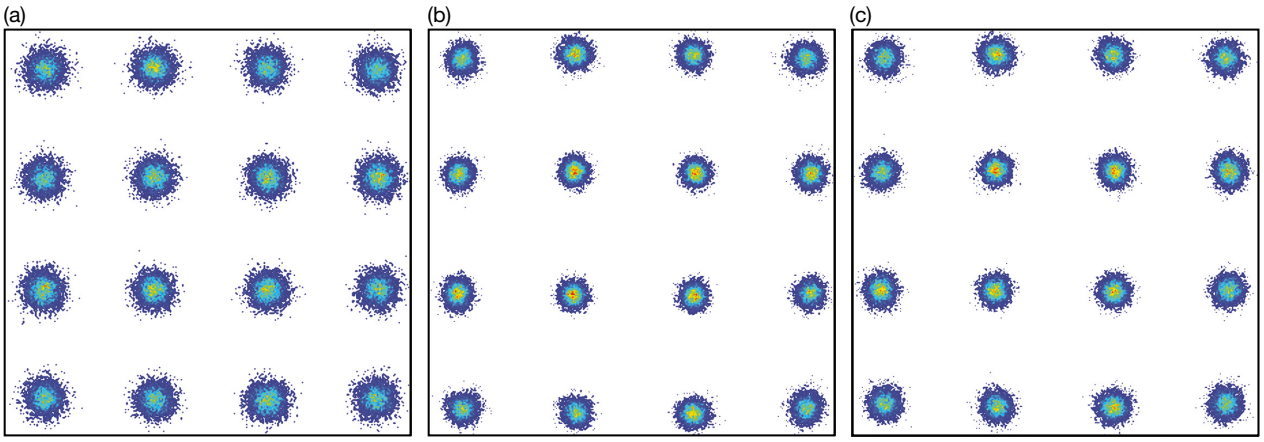

Figure 13. 10-Gb/s 16-QAM constellation diagrams for beam-steering angles: (a) −35°, (b) 0°, (c) 35°. (Reproduced from Ref. 16.)

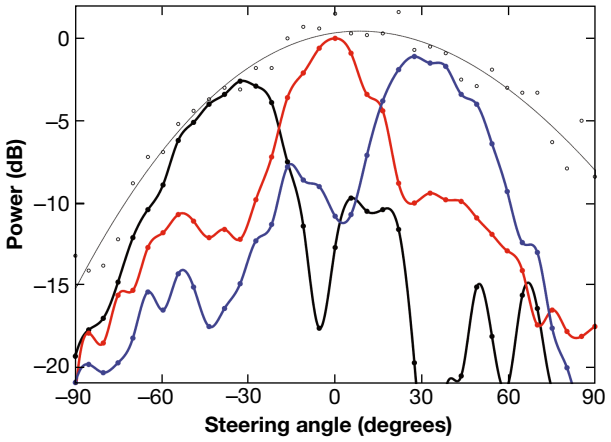

Figure 14. Beam patterns for steering angles of −35° (black), 0° (red), and 35° (blue). The pattern of the first element (dots with black fit) shows the radiation pattern envelope. (Reproduced from Ref. 16.)

steering, the EVM of the demodulated constellation was 7.7%, and at 35° steering the EVM was 6.1%.

To validate the steering behavior, a far-field radiation pattern was measured and shown in Fig. 14 for a carrier frequency of 85 GHz with steering angles of −35°, 0°, and 35°. The single-element radiation pattern serves as the envelope for the steered array.

CONCLUSION

By combining electronic and photonic technologies in high-data-rate communications systems, the relative benefits of each technology can be used to develop systems more capable than either technology can support alone. Compact, high-data-rate systems are made possible by the wide-signal bandwidths available at mm-wave carrier frequencies, the favorable propagation characteristics of mm-wave radiation at W-band, and the compact physical size of mm-wave components and antennas. Along with these benefits, the ability of photonics to lift bandwidth restrictions on the upconversion and downconversion stages, as well as to generate spectrally pure signals, allows the use of high-modulation format signals that can further increase the data rate. Future mm-wave communications systems are anticipated to achieve data rates exceeding 100 Gb/s over distances of tens of kilometers or more.

The mm-wave front end requires power gain and aperture gain to achieve communications over appreciable distances. Current mm-wave amplifier technology using GaAs and GaN can achieve output powers of more than 2.5 W through W-band, and this number will increase with improved device technology and power-combining techniques. Used with reflecting antenna systems such as Cassegrain or Gregorian reflectors, such amplifier technology allows data rates of multiple gigabits per second to be easily transmitted over tens of kilometers. Ongoing research in mm-wave phased arrays shows significant promise for achieving the same power-aperture using numerous elements in a significantly smaller aperture footprint, which will allow the use of mm-wave communications systems over large distances on small platforms.

Although the bandwidth of photonic technologies remains significantly greater than that of electronics, current research and development in photonics aims to increase the maximum operating frequency of photonic components. Photodiodes and electro-optic modulators operating at frequencies up to 40 GHz are widely available, and those operating up to 100 GHz are becoming commercially available. Further improvements in photonic component efficiency will enable mm-wave communications at frequencies well beyond 110 GHz. Even with these developments in component technology, cost and integration are likely to remain the key challenges for mm-wave systems using photonics. Integrated photonics, in which multiple photonic components are combined on a single substrate, can enable systems that feature a much less pronounced electronic–photonic interface than in current systems. Combined with integrated mm-wave electronics advancements, future mm-wave wireless systems with integrated photonics can offer high performance in small form factors at low powers and reasonable costs.

REFERENCES

[1]Currie, N. C., and Brown, C. E., *Principles and Applications of Millimeter-Wave Radar*, Artech House, Boston (1987).
[2]Taylor, G. B., Carilli, C. L., and Perley, R. A. (eds.), *Synthesis Imaging in Radio Astronomy II*, Astronomical Society of the Pacific, San Francisco (1999).
[3]Gross, M. C., Callahan, P. T., Clark, T. R., Novak, D., Waterhouse, R. B., and Dennis, M. L., "Tunable Millimeter-Wave Frequency Synthesis up to 100 GHz by Dual-Wavelength Brillouin Fiber Laser," *Opt. Express* **18**(13), 13321–13330 (2010).
[4]Nanzer, J. A., Callahan, P. T., Dennis, M. L., Clark, T. R., Novak, D., and Waterhouse, R. B., "Millimeter-Wave Wireless Communication Using Dual-Wavelength Photonic Signal Generation and Photonic Upconversion," *IEEE Trans. Microwave Theory Tech.* **59**(12), 3522–3530 (2011).
[5]Clark, T. R., O'Connor, S. R., and Dennis, M. L., "A Phase-Modulation I/Q-Demodulation Microwave-to-Digital Photonic Link," *IEEE Trans. Microwave Theory Tech.* **58**(11), 3039–3058 (2010).
[6]McKenna, T. P., Nanzer, J. A., and Clark, T. R., "Photonic Down-converting Receiver Using Optical Phase Modulation," in *Proc. IEEE MTT-S Int. Microwave Symp.*, Tampa Bay, FL, pp. 1–3 (2014).
[7]McKenna, T. P., Nanzer, J. A., Dennis, M. L., and Clark, T. R., "Fully Fiber-Remoted 80 GHz Wireless Communication with Multi-Subcarrier 16-QAM," in *Proc. IEEE Photonics Conf.*, San Francisco, CA, pp. 546–577 (2012).
[8]McKenna, T. P., Nanzer, J. A., and Clark, T. R., "Experimental Demonstration of Photonic Millimeter-Wave System for High Capacity Point-to-Point Wireless Communications," *J. Lightwave Technol.* **32**(20), 3588–3594 (2014).
[9]Cox, C. H. III, Ackerman, E. I., Betts, G. E., and Prince, J. L., "Limits on the Performance of RF-over-Fiber Links and their Impact on Device Design," *IEEE Trans. Microwave Theory Tech.* **54**(2), 906–920 (2006).
[10]Gopalakrishnan, G. K., Moeller, R. P., Howerton, M. M., Burns, W. K., Williams, K. J., and Esman, R. D., "A Low-Loss Downconverting Analog Fiber-Optic Link," *IEEE Photon. Technol. Lett.* **43**(9), 2318–2323 (1995).

[11]Karim, A., and Devenport, J., "High Dynamic Range Microwave Photonic Links for RF Signal Transport and RF-IF Conversion," *J. Lightwave Technol.* **26**(15), 2718–2724 (2008).
[12]Juodawlkis, P. W., Hargreaves, J. J., Younger, R. D., Titi, G. W., and Twichell, J. C., "Optical Down-Sampling of Wide-Band Microwave Signals," *J. Lightwave Technol.* **21**(12), 3116–3124 (2003).
[13]Kim, J., Park, M. J., Perrott, M. H., and Kärtner, F. X., "Photonic Subsampling Analog-to-Digital Conversion of Microwave Signals at 40-GHz with Higher than 7-ENOB Resolution," *Opt. Express* **16**(21),16509–16515 (2008).
[14]McKenna, T. P., Nanzer, J. A., Dennis, M. L., and Clark, T. R., "Mixerless 40 GHz Wireless Link Using a Photonic Upconverting Transmitter and a Photonic Downsampling Receiver," in *Proc. IEEE MTT-S International Microwave Symp.*, Seattle, WA, pp. 1–3 (2013).
[15]Proakis, J. G., *Digital Communications*, 4th Ed., McGraw, New York (2001).
[16]McKenna, T. P., Nanzer, J. A., and Clark, T. R., "Photonic Beamsteering of a Millimeter-Wave Array with 10-Gb/s Data Transmission," *IEEE Photon. Technol. Lett.* **26**(14), 1407–1410 (2014).

THE AUTHORS

Timothy P. McKenna is a member of the Associate Professional Staff in the Microwave Photonics Section of the Air and Missile Defense Sector. He worked across many disciplines and was involved with the system design and demonstrations described in this article. **Jeffrey A. Nanzer** is a member of the Senior Professional Staff and Section Supervisor in the Air and Missile Defense Sector. He provided expertise in mm-wave systems and technology. **Thomas R. Clark Jr.** is a member of the Principal Professional Staff and Group Supervisor in the Air and Missile Defense Sector. He contributed expertise in communications and photonics system design and provided future directions for this research. For further information on the work reported here, contact Timothy McKenna. His e-mail address is timothy.mckenna@jhuapl.edu.